Polymer Vol. 38 No. 7, pp. 1513–1519, 1997

0032-3861/97/$17.00 + 0.00

PII: S0032-3861(96)00675-1

polymer papers

Coil dimensions and conformation of macromolecules in aqueous media from flow field-flow fractionation/multi-angle laser light scattering illustrated by studies on pullulan

Ulrich Adolphi and Werner-Michael Kulicke*
Institut für Technische und Makromolekulare Chemie, Universität Hamburg, Bundesstraße 45, 20146 Hamburg, Germany
(Received 6 November 1995; revised 29 April 1996)

For a comprehensive description of the steric structure of macromolecules, which includes molecular shape as well as coil density and flexibility, a novel analytical technique for aqueous systems is introduced. The reliability of the method is illustrated by investigations on narrowly distributed pullulan standards in the molar mass range from 10^5 to 10^6 g mol^{-1}. Hydrodynamic information (D, R_D) was yielded by flow field–flow fractionation, while simultaneous scattering experiments delivered the corresponding 'static' dimension R_G and molar mass M. The observed asymmetry-factor was $R_G/R_D = 1.7$. With increasing molar mass the mean coil density ρ_{Pol} decreased from 19.1 to 2.6 mg ml^{-1} and the calculated persistence lengths l_P increased, ranging from 1.4 to 3.1 nm. The results were found to be in good agreement with literature data and confirm the analytical potential of the applied technique.

(Keywords: asymmetry-factor; persistence length; overlap concentration)

INTRODUCTION

Properties of polymer solutions, such as viscosity, elasticity and the ability to exhibit mesophases, are mainly dominated by the conformation and dimension of the macromolecules[1–4]. The underlying steric structure may significantly change for a given polymer with variations in solvent composition, temperature, concentration or chain length[5–8]. For a more detailed understanding of molecular interactions, as well as for many technical applications, a knowledge of the actual molecular shape is of great importance. Regular and simple geometrical shapes with well-defined boundary surfaces are formed by just a few macromolecules, e.g. latex particles. In contrast, most dissolved macromolecules have to be described in terms of an asymmetrical, expanded and inhomogeneous coil[9–11].

Considering the complex nature of polymer conformations the root mean square radius R_G, which is obtained by static scattering experiments, serves as a practical overall parameter for coil dimensions,

$$R_G \equiv \langle R_G^2 \rangle^{1/2} = \left(\frac{1}{2N} \cdot \sum_i^N \sum_{j \neq i}^N \langle r_{ij}^2 \rangle \right)^{1/2} \quad (1)$$

for a chain with N segments and a distance r_{ij} between segments i and j. The effective hydrodynamic radius of a macromolecule R_H represents another useful quantity for polymer dimensions. Depending on the method by which R_H is obtained, one distinguishes between the Stokes-radius R_D (from diffusion measurements) and the Einstein-radius R_η (from viscosimetry).

$$R_H \equiv \langle R_H^{-1} \rangle^{-1} = \left(\frac{1}{2N} \cdot \sum_i^N \sum_{j \neq i}^N \langle r_{ij}^{-1} \rangle \right)^{-1} \quad (2)$$

Because of their different definitions R_G and R_H normally do not coincide: larger chain dimensions are more strongly weighted by R_G while R_H is dominated by shorter interchain distances. Consequently, depending on which radius is used for calculation, significant deviations are observed for the volume occupied by the polymer ($V \sim R^3$) and thus for the overlap concentration c^*[8,14,15].

An inherent characteristic of the scalar quantities R_G and R_H is the fact that they each give just a mean one-dimensional and time-averaged impression of the true anisotropic extension of a fluctuating polymer chain. Thus, it has been recognized that macromolecules cannot be described properly by just one of these radii[16]. Conversely, a combination of both quantities enables a detailed insight into the molecular architecture. For this purpose the shape-factor or asymmetry-factor p is defined[17,18]. Values of p vary from 0.778 for ideal, homogeneous spheres up to >2 for extended coils and prolate ellipsoids (*Figure 1*).

$$p = \frac{R_G}{R_H} \quad (3)$$

* To whom correspondence should be addressed

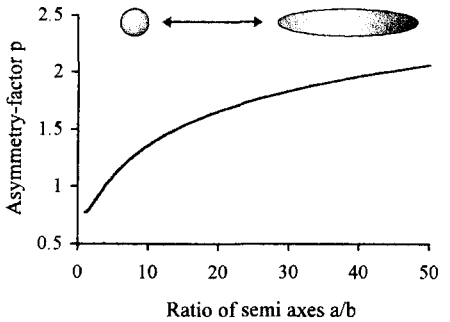

Figure 1 Dependence of the asymmetry-factor $p (= R_G/R_H)$ on the ratio of the semiaxes a/b. Calculations were carried out according to the formulae given in *Table 1*

For ellipsoids the ratio of the main semiaxes can be calculated directly from p (*Table 1*). A major requirement for the correct determination of p is in the equality of the experimental conditions (solvent, temperature, concentration, primary treatment such as heating or filtration, shear stress, etc.) when determining R_G and R_H. In particular, attention has to be paid to the polydispersity of the sample[19,20]. For a polydisperse polymer distinct analytical techniques yield different moments of the corresponding radius distribution. Erroneous interpretations will result, e.g., from a comparison of a z-average R_G with an η-average R_H.

In this study a novel analytical technique[21–23] will be introduced for the characterization of polymer dimensions in aqueous media. Independent of the sample's polydispersity R_G and R_H of corresponding monodisperse fractions will be obtained within a *single* measurement. There are no restrictions to sample composition or molecular shape. The experimental setup employed consists of a flow field-flow fractionator (F^4), the outlet of which is coupled on-line to a multi-angle laser light scattering (MALLS) photometer and differential refractometer (DRI). The principles of F^4/MALLS/DRI measurements and data evaluation are demonstrated on the biopolymer pullulan[24]. This extracellular polysaccharide, which is produced by the fungus *Aureobasidium pullulans*, is composed exclusively of linearly linked α-D-glucose residues. Because of its good solubility in water pullulan is often used as a calibration standard for liquid chromatography. In this study a set of three pullulan standards were examined by F^4/MALLS/DRI to obtain molar masses, root mean square radii and diffusion coefficients. From these primary quantities root mean square end-to-end distances, hydrodynamic radii and overlap concentrations were calculated, along with asymmetry-factors and the corresponding ellipsoidal dimensions. In addition, consideration is given to whether the observed scattering functions may be taken into account for description of the macromolecular shape. Beside the conformational characterization, the flexibility of the polymer chain is also estimated in terms of the persistence length. In order to estimate the reliability and analytical potential of the applied technique, experimental data are compared with known values from literature.

EXPERIMENTAL

Figure 2 shows a scheme of the experimental setup. The F^4/MALLS/DRI apparatus used consists of a diffusion-driven separation unit and a tandem detection unit. In flow field-flow fractionation (F^4) separation is achieved by means of two flowstreams passing through a flat channel perpendicular to each other. The cross flow, $\dot{V}_x$, forces all particles within the channel towards the accumulation wall and gives rise to a concentration profile characteristic for each species. The smaller the diffusion coefficient, D, of the species, the closer their mean distance, x, from the accumulation wall. The second flow, the channel flow, $\dot{V}_z$, exhibits a parabolic velocity profile which amplifies the small differences in x to larger distances z along the channel axis (see *Figure 2*). Concentration gradient and velocity gradient act together and give rise to separation according to different diffusion coefficients. For well-retained species a good approximation of D may be directly calculated from the retention time t_R, the channel height w, and the applied flow rates:

$$D = \frac{w^2}{6t_R} \times \frac{\dot{V}_x}{\dot{V}_z} \tag{4}$$

A more comprehensive description of the separation mechanism in F^4 is beyond the scope of this basic approach and is given in detail elsewhere[25–27]. The FFfractionator employed was a model F-1000 from Fractionation Inc. with nominal channel dimensions as follows: 254 μm high, 28.5 cm long and 2.5 cm wide. The accumulation wall was covered with a YM-10 membrane of regenerated cellulose. Sample loops from 25 to 100 μl were applied. Channel flow, $\dot{V}_z$, was provided by a constaMetric 3200 HPLC-pump from LDC Analytical (Rivera Beach, USA) with a constant flow-rate of 0.54 ml min^{-1}. The circulating cross-flow, $\dot{V}_x$, was supplied by a double piston pump RC 10 from Reichelt Chemietechnik with flow rates from 0.33 to 2 ml min^{-1}. Flow rates were determined gravimetrically. Carrier solution was purified on-line by filtration (0.2 μm) and degassed by a degasser, model A1010 from Knauer.

Each volume fraction eluted from the F^4-channel passes through a flow cell, where the scattered light from an incident laser beam is detected simultaneously at 15 fixed angles (from 21.5° to 148.4°). A DAWN F light

Table 1 Root mean square radii R_G and hydrodynamic radii R_H for simple geometrical shapes[10–13]

	Sphere (radius r)		Prolate ellipsoid (semiaxes $b < a$)	Rigid rod (diameter $2r \ll$ length l)
	Hollow	Solid	Solid	Solid
R_G	r	$\sqrt{\frac{3}{5}}r$	$\sqrt{\frac{1}{5}(a^2+2b^2)}$	$\sqrt{\frac{1}{12}\times l^2+\frac{1}{2}\times r^2}$
R_H	r	r	$a(1-(b/a)^2)^{0.5}\times\ln\left[\left(\frac{1+(1-(b/a)^2)^{0.5}}{b/a}\right)\right]^{-1}$	$l\left[10.54+4.2\left(\left(\ln\frac{l}{r}\right)^{-1}-0.39\right)^2+7.4\left(\left(\ln\frac{l}{r}\right)^{-1}-0.34\right)^2\right]^{-1}$

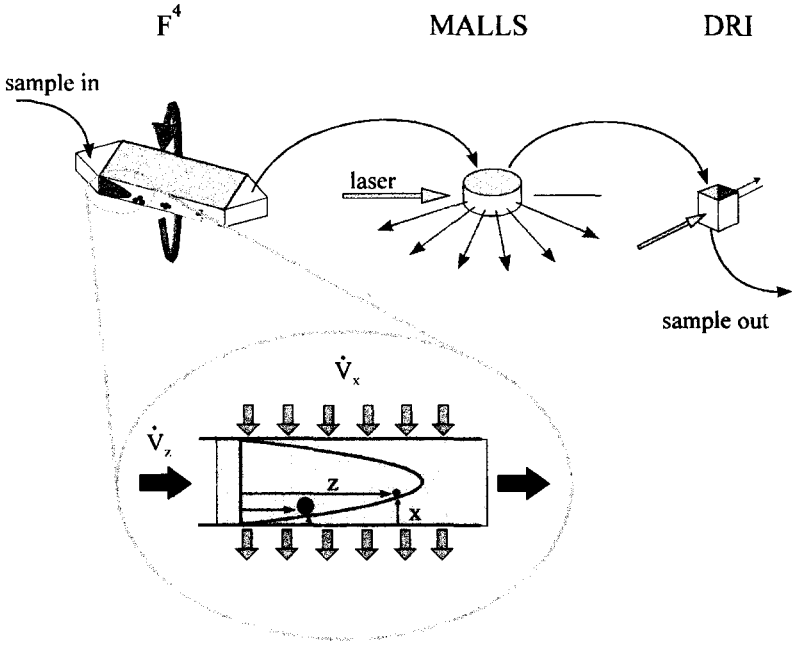

Figure 2 Schematic view of the experimental setup consisting of flow field-flow fractionation (F^4), multi-angle laser light scattering (MALLS) and differential refractive index detection (DRI). The separation process within the F^4-channel is shown in detail

scattering photometer from Wyatt Technology Corp. with a linear polarized He-Ne laser ($\lambda_0 = 633$ nm) and a K5 cell was used for measurements. Data were received and analysed by ASTRA 2.11, a software package supplied with the photometer.

If ideal separation conditions are assumed, the polydispersity within the examined volume fractions may be neglected; otherwise weight-average molar masses M_w and z-average radii R_{Gz} are obtained for each volume fraction. Light scattering data were evaluated by a first-order extrapolation to zero scattering angle according to ZIMM as represented by the following equation,

$$\frac{Kc}{R_\vartheta} = \frac{1}{P_\vartheta} \times \left(\frac{1}{M_w} + 2A_2c + \ldots\right) \quad (5)$$

where R_ϑ is the reduced scattering intensity at the angle ϑ and P_ϑ denotes the scattering function, from which R_{Gz} is calculated[28]. A_2 denotes the second virial coefficient of the respective polymer–solvent system. The optical contrast factor κ considers the specific refractive index increment (dn/dc), the solvent refractive index n_0, and the vacuum wavelength of the incident light λ_0.

$$K = \frac{4\pi^4 n_0^2}{N_A \lambda_0^4} \times \left(\frac{dn}{dc}\right)^2 \quad (6)$$

for each volume fraction the actual polymer concentration c was determined by means of a differential refractometer, model RI SE-51 from Showa Denko. The refractometer signal intensity I is directly proportional to c and (dn/dc). The computed concentration is therefore inversely proportional to the specific refractive index increment.

$$c \propto I\left(\frac{dn}{dc}\right)^{-1} \quad (7)$$

According to equations (6) and (7) it should be noted that the product, K and c, in equation (5) is just linearly related to (dn/dc), resulting in reduced influence of erroneous (dn/dc) values compared with concentration determination, e.g. by u.v.-detection[29]. Because of the dilution associated with separation, polymer concentrations are normally very low within the scattering volume ($<10^{-5}$ g ml^{-1}). Therefore, the second term of the sum in equation (5) may be neglected for small values of A_2, without any significant effects on the results (see below).

Narrowly distributed ($M_w/M_n < 1.1$) pullulan standards with nominal molecular weights 2×10^5 g mol^{-1} (P200), 4×10^5 g mol^{-1} (P400) and 1.6×10^6 g mol^{-1} (P1600) were received from Polymer Standards Service (Mainz, Germany). Deionized and distilled water with 0.1 mol l^{-1} sodium nitrate and 0.02% (w/w) sodium azide (purchased from Merck) was used as solvent as well as a carrier solution. Stock solutions were prepared without mechanical or thermal agitation and shown to be stable over a period of several months. Concentrations of the injected solutions ranged from 1 to 5 mg ml^{-1}. Calculations were carried out with $(dn/dc) = 0.147$ ml g^{-1} and $A_2 = 2.5 \times 10^{-4}$ ml × mol g^{-2} (ref. 30).

RESULTS AND DISCUSSION

For a given sample the elution profile in F^4 depends on the applied cross flow. In the case of sample P400 for example, it was found that optimum flow rates are in the range from about 0.5 to 0.7 ml min^{-1}, as demonstrated in *Figure 3*. At lower flow rates separation power is sacrificed unnecessarily and rather narrow peaks are obtained, while at higher flow rates detectability decreases due to increasing dilution. As shown by equation (4), retention time of a species is inversely proportional to its diffusion coefficient. At fixed flow rates, retention time significantly increases with increasing molar mass ($D \propto M^{-\text{const}}$), accompanied by a growth in band width and a fall in concentration. Thus, in the following investigation of P200, P400 and P1600 cross-flow rates of 0.83, 0.67 and 0.50 ml min^{-1}, respectively, were applied. It must be emphasized that the

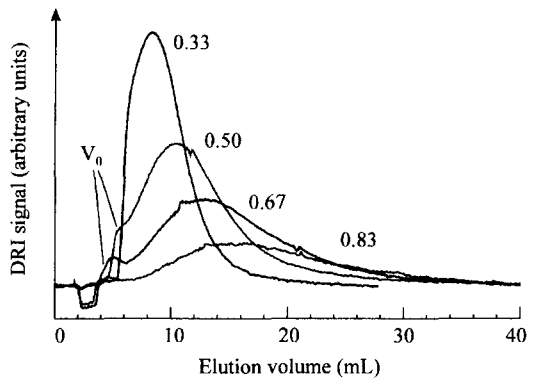

Figure 3. Elution profiles of sample P400 obtained at different cross flow rates (from 0.33 to 0.83 $ml^{-1}\,min^{-1}$). The region of the 'void volume' V_0 is also inserted

Table 2 Results from F^4 measurements. Diffusion coefficients D and radii R_D have been calculated for peak maxima at retention time t_R. Accuracy is ±5%

	$\dot{V}_x$ (ml min^{-1})	t_R (s)	D ($cm^2\,s^{-1}$)	R_D (nm)
P200	0.83	589	2.73×10^{-7}	8.2
P400	0.67	844	1.52×10^{-7}	14.6
P1600	0.50	1411	0.68×10^{-7}	32.6

calculated results are independent of the cross flow. The elution volumes of the respective peak maxima were corrected by the so-called 'void volume' V_0, which represents the first possible elution of any particles, and converted to a time scale by the applied channel flow. Diffusion coefficients D are simply related to Stokes-radii R_D,

$$R_D = \frac{k_B T}{6\pi\eta D} \tag{8}$$

with solvent viscosity η and thermal energy $k_B T$. R_D is a measure of the hydrodynamic interaction or friction between polymer and solvent, and therefore it is possible to correlate R_D via the friction coefficient f with the 'effective surface area' A of the molecule[31].

$$R_D \propto \frac{k_B T}{D} = f \approx 6\pi\eta\sqrt{\frac{A}{4\pi}} \tag{9}$$

It should be noted that the Stokes-radius, R_D, estimated by diffusion measurements is not necessarily identical with the above mentioned Einstein-radius, R_η, a hydrodynamic radius determined by viscosimetry. R_η is related to the product of molar mass M and Staudinger-index, $[\eta]$, divided by the Avogadro number, N_A:

$$R_\eta = \sqrt[3]{\frac{3M[\eta]}{10\pi N_A}} \tag{10}$$

The hydrodynamic properties calculated for P200, P400 and P1600 in the peak maxima are summarized in *Table 2*. *Table 3* shows the corresponding data from the light scattering measurements. Molar masses and root mean square radii calculated at the peak maxima; mean values over the whole peak area are also specified. It can be seen, as mentioned above, that due to the very low concentrations the second virial coefficient exerts no significant influence on the results. Likewise the indicated uncertainty of the calculated molar masses and radii can be attributed to the very low concentrations. The uncertainty diminishes with increasing coil dimensions, thus scattering intensity. Worthy of particular note is a significant deviation between nominal and measured molar mass for sample P1600. This feature is attended by a distinct 'loss' of sample during separation, this means that about 30% of the injected material does not elute until the cross flow is switched off. A possible explanation for this phenomenon is given below in connection with the calculated overlap concentration.

In contrast to the effective hydrodynamic radii R_D and R_η, which are complex and poorly understood quantities, not least owing to the deformation of segment distribution during molecular motion[16,32], the 'static' radius R_G may serve as an expressive description of a polymer coil. By replacing the intersegment distance r_{ij} in equation (1) by the segment's distance from the coil's centre of gravity r_{i0}, a clear approach to coil dimensions is possible. Applying the model of a Gaussian-like segment distribution, it can be shown that 91.7% of all segments are found within a distance R_G from the centre of gravity while the remaining segments are up to 2.25 times as far apart. (The index G in R_G comes from reference to the centre of *gravity*[33]. The frequently used term 'radius of *gyration*' for denoting R_G is in a strict sense correct only for two-dimensional objects with the axis of rotation perpendicular to the plane located in their centre of gravity.) Depending on the particle's shape and density R_G is directly related to its mass, M. For homogeneous spheres M increases with the cube of R_G, in the case of linear, undisturbed chains M is proportional to the square of R_G, and for thin rods there is a linear relationship between M and R_G. Thus, the exponent ν of an R_G–M relationship is a direct measure of the polymer conformation. Apart from the shape of a molecule its density also contributes to ν: for flexible polymer coils a value of $\nu = 0.5$ describes the non-draining limit, while the free-draining limit is theoretically given by $\nu = 0.66$. Similar relationships, but with the exponent having a negative sign, exist for the dependence of the diffusion coefficient on molar mass. The following are some of the relationships that have already been published for pullulan in water:

$R_G = 1.91 \times 10^{-2} M^{0.56}$ and $D = 1.76 \times 10^{-4} M^{-0.54}$

(according to ref. 30), and

Table 3 Results from MALLS measurements. Molar masses M and radii R_G have been calculated for the volume fractions corresponding to the peak maxima (see *Table 2*) and also over the whole peak area. Two different virial coefficients have been applied for the purpose of comparison. The errors indicated can be attributed to low scattering intensities owing to very low concentrations, particularly for P200

	$A_2 = 2.5 \times 10^{-4}$ ml mol g^{-2}		$A_2 = 0$ ml mol g^{-2}				
	M_W (g mol^{-1})	R_{G_z} (nm)	M_w (g mol^{-1})	R_{G_z} (nm)	M_w/M_n	M_{Peak} (g mol^{-1})	$R_{G\,Peak}$ (nm)
P200	$(1.7 \pm 0.3)\,10^5$	15.5 ± 12.8	$(1.7 \pm 0.3)\,10^5$	15.5 ± 12.8	1.02	$(1.7 \pm 0.2)\,10^5$	15.3 ± 10.1
P400	$(3.5 \pm 0.3)\,10^5$	23.4 ± 6.6	$(3.5 \pm 0.3)\,10^5$	23.4 ± 6.6	1.02	$(3.7 \pm 0.2)\,10^5$	23.7 ± 5.5
P1600	$(9.0 \pm 0.9)\,10^5$	56.1 ± 5.4	$(9.0 \pm 0.9)\,10^5$	56.0 ± 5.4	1.05	$(9.7 \pm 0.6)\,10^5$	54.6 ± 4.9

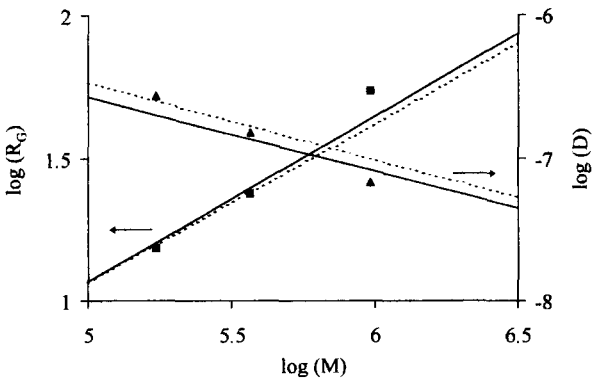

Figure 4 Double logarithmic plot with the values obtained for M, R_G (squares) and D (triangles) for P200, P400 and P1600. The linear R_G–M and D–M relationships determined by Douglas and Freed[31] (dotted line) and Kato *et al.*[34] (solid line) are also shown

$$R_G = 1.47 \times 10^{-2} M^{0.58} \quad \text{and} \quad D = 1.07 \times 10^{-4} M^{-0.52}$$

(according to ref. 34).

Values for ν of 0.56 and 0.58 indicate a partially expanded conformation of the dissolved pullulan. As shown in *Figure 4* the values of M, D and R_G obtained in this study are in good agreement with these relationships (no average-index is used because the values refer to monodisperse volume fractions at peak maxima).

For linear chains the root mean square end-to-end distance r_∞ may be calculated from R_G and ϵ:

$$r_\infty \equiv \langle r_\infty^2 \rangle^{0.5} = \left(6R_G^2 \left(1 + \frac{5}{6} \times \epsilon + \frac{1}{6} \times \epsilon^2 \right) \right)^{0.5} \qquad (11)$$

The expansion coefficient ($\epsilon = 2\nu - 1$) considers the excluded volume for a disturbed coil. For an undisturbed coil ϵ would approach zero. The mean square end-to-end distance r_∞^2 of a flexible, undisturbed polymer chain is directly proportional to its persistence length l_P.

$$l_P = \frac{r_\infty^2}{2 \times DP \times l_{Mon}} \qquad (12)$$

$DP = M/M_{Mon}$ denotes the degree of polymerization and l_{Mon} is the length of a monomer unit, with the contour length of the chain $l_{cont} = DP \times l_{Mon}$. The persistence length, l_P, is a widely used measure for the stiffness of the polymer backbone and indicates the distance along the chain over which the orientation of any segment persists. It can be seen from equation (12) that for undisturbed chains, where $r_\infty^2 \propto M(\nu = 0.5)$, l_P is a constant for each polymer type. *Table 4* shows the values obtained for root mean square end-to-end distance, contour length and persistence length of the pullulans investigated. For calculation of l_P, the coil expansion indicated by $\nu \cong 0.57$ respective $\epsilon \cong 0.14$ was neglected and an undisturbed conformation was assumed. $l_{Mon} = 0.479$ nm was taken as the effective length of the glycopyranose repeat unit ($M_{Mon} = 162\,g\,mol^{-1}$)[19]. Hence the persistence lengths calculated, ranging from 1.4 to 3.1 nm, correspond to one or two maltotriose units, which agrees reasonably well with recently reported data[35]. The assumption of undisturbed dimensions is contrasted by an observed increase of l_P with M, which indicates $\nu \neq 0.5$. The high flexibility of the polymer backbone is shown by large values of $l_{cont}/l_P \gg 1$.

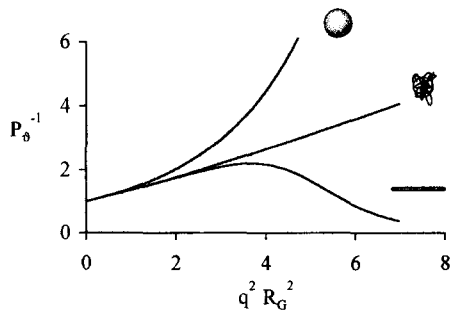

Figure 5 Calculated reciprocal scattering functions for solid spheres, ideal coils and rigid rods. Calculations were based on particles with $R_G = 100$ nm with $n = 1.33$ and $\lambda_0 = 633$ nm

Additional information about the flexibility and shape of the polymer chain may be obtained from the scattering function P_ϑ. Regardless of molecular shape, P_ϑ yields root mean square radii by extrapolation of its slope to small scattering vectors q. For large values of q times R_G, the scattering function P_ϑ exhibits a significant dependence on molecular shape (*Figure 5*) and polydispersity of the sample. Working with F^4/MALLS/DRI enables monodispersity to be assumed for each volume fraction under investigation. Thus, only molecular shape and flexibility should influence the curvature of P_ϑ for large q times R_G products. Unfortunately, the samples investigated are too small for a clear statement on the molecular architecture. In *Figure 6* the measured scattering function for P1600 at the peak maximum is contrasted with theoretically predicted scattering functions of expanded coils/semiflexible rods with different ratios l_{cont}/l_P. The detector signals are somewhat noisy owing to the weak scattering intensity, which results from the very low concentration. A reasonable comparison of experimental with theoretical scattering functions would require larger particle dimensions R_G and scattering vectors q (at least $q^2R_G^2 > 4$; compare *Figure 5*). The respective scattering functions shown in *Figure 6* were estimated by means of the following equation[36].

$$P_\vartheta = e^w \cdot \sum_{n=0}^{\infty} \left\{ \frac{(-w)^n}{n!} \times F((w+n)x) \right\} \qquad (13)$$

$$\text{with } w = q^2 R_G^2 (x + 3F(x) - 3)^{-1}$$

$$\text{and } F(x) = 2x^2(e^{-x} - 1 + x)$$

and x denotes the ratio l_{cont}/l_P and q is defined as $q = 4\pi/\lambda \sin(\vartheta/2)$.

In the case of simple geometrical shapes with a defined

Table 4 Chain dimensions calculated from light scattering data at peak maxima assuming undisturbed conformation ($\epsilon = 0$)

	DP	l_{cont} (nm)	r_∞ (nm)	l_P (nm)	l_{cont}/l_P
P200	1060 ± 120	510 ± 60	37.5 ± 24.5	1.4 ± 0.7	370 ± 120
P400	2280 ± 120	1090 ± 60	58.1 ± 13.5	1.6 ± 0.3	700 ± 110
P1600	5980 ± 360	2890 ± 170	133.7 ± 12.0	3.1 ± 0.2	920 ± 60

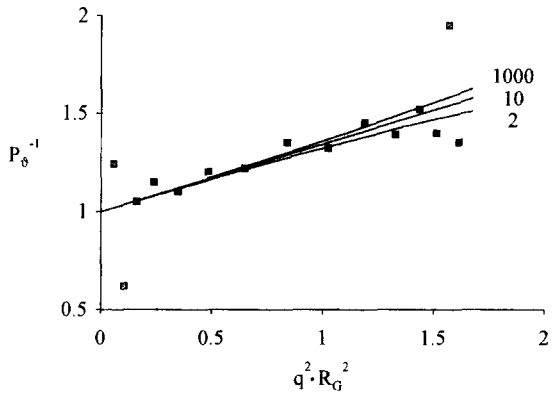

Figure 6 Measured reciprocal scattering function of P1600 at peak maxima (squares) compared with theoretical scattering functions of expanded coils/semiflexible rods with l_{cont}/l_P ranging from 2 to 1000. The first, second and last squares were not included in calculations

boundary surface and homogeneous mass distribution the radii R_G and R_H (here is $R_D = R_\eta$) may be calculated from the external particle dimensions (*Table 1*). It can be seen that the ratio R_G/R_H (that is the asymmetry factor p) increases with decreasing density (solid sphere–hollow sphere) and with increasing asymmetry (sphere–ellipsoid; *Figure 1*). For an undisturbed coil with a spherical, but inhomogeneous conformation theoretical values of p have been calculated as $R_G/R_D = 1.28$ and $R_G/R_\eta = 1.37$[10] and are predicted to decrease with increasing polydispersity[18]. Other published p-values range from 0.9 to 1.9[17,37,38], depending on the theoretical model applied or the experimental conditions chosen. For pullulan in water values of 1.4–1.7 have been found[30,34]. In this study we observed p-values of 1.62 to 1.86, which can be correlated with the effective shape of a prolate ellipsoid with the major semiaxis a being as much as 19–32 times large than the minor semiaxes b (*Table 5*). The specified quantities of a and b merely demonstrate the ellipsoidal shape in qualitative molecular dimensions. They should not be taken literally, because unfortunately the same problem that occurs with the exponent ν applies to the dimensionless parameter p, i.e. the particular contributions of density and asymmetry cannot be separated from each other. For a closer approach to the real molecular architecture the density within the polymer coils has to be taken into account.

Within an ideal polymer coil the segment density reaches a maximum at the centre of gravity and decreases continuously with increasing distance. The mean density, ρ_{Pol}, given by the ratio of coil mass to coil volume, decreases with increasing molar mass:

$$\rho_{Pol} = \frac{m_{Pol}}{V_{Pol}} = \frac{M/N_A}{4/3\pi R_G^3} \propto \frac{M}{R_G^3} \propto \frac{M}{M^{3\nu}} = M^{1-3\nu} \quad (14)$$

The 'static' radius R_G in the above equation may be substituted by the hydrodynamic radius R_D or R_η. (Actually equation (8) results from equation (14) by applying the Einstein relationship $\rho_{Pol} = 2.5/[\eta]$[39,40].) It has to be pointed out that the apparent density obtained by calculations, such as shown by equation (14), will be larger than the true value since $R_H < R_G < R_{true}$, with R_{true} being the maximum distance of a segment from the centre of gravity ($R_{true} \cong 2.25 \times R_G$, see above). In a first approximation, neglecting long-range interactions and the non-cubic shape of macromolecules, the mean density ρ_{Pol}, is about equal to the critical overlap concentration c^*, at which isolated coils begin to touch each other. There are different approaches[41] describing c^*, but in any case it has to be borne in mind that experimental results[8,14,15] and also theoretical considerations[42] indicate intermolecular interactions even below such values of c^*. As can be seen from the data in *Table 5*, the mean segment density within the pullulan coils, and thus the corresponding overlap concentration, decreases significantly with increasing molar mass. In the case of P1600, ρ_{Pol} amounts to just a few mg ml^{-1}. According to the primary concentration of about 1 mg ml^{-1}, the overlap concentration c^* may have been exceeded within the F^4-channel during measurements. As a consequence, large polymer coils may become entangled with each other and are retained inside the F^4-channel due to the applied field of force until the cross flow is switched off[43]. This would explain the 'loss' of sample as well as the low molar mass compared to the distributor's declaration (see above).

CONCLUSIONS

The novel analytical method F^4/MALLS/DRI has been shown to be applicable to the conformational characterization of pullulan dissolved in aqueous media. The results obtained in this study confirm that the linear polysaccharide dissolved in water behaves like a highly flexible polymer in a good solvent. Calculated values of D, R_D, R_G, l_P, c^* for the corresponding M are in good agreement with literature data. Thus, a new method is available for the steric characterization of even small polymers, where the scattering function contains no information about molecular shape and flexibility. The experimental setup ensures that the corresponding hydrodynamic and 'static' quantities are obtained from the same monodisperse volume fraction, independently of sample composition. Furthermore, it has been shown that owing to the low polymer concentration employed the second virial coefficient A_2 has neglectable influence on the light-scattering results. An unusual elution behaviour observed for the high molar mass sample P1600 has been explained in terms of cross-flow induced entanglements. A programmed cross flow, which

Table 5 Shape and density parameters calculated from combined F^4 and MALLS results

	Shape				ρ_{Pol} (mg ml^{-1})	
	R_G/R_D	a/b	a (nm)	b (nm)	Applying R_D	Applying R_G
P200	1.86 ± 1.26	31.8	35.1	1.1	123.6	19.1
P400	1.62 ± 0.40	18.6	52.1	2.8	46.7	10.9
P1600	1.67 ± 0.18	20.7	122.1	5.9	11.1	2.6

decreases continuously during the measurement, would possibly avoid such 'overloading' effects. This phenomenon will be subjected to further investigation in our laboratory.

ACKNOWLEDGEMENTS

This work was supported by the Deutsche Forschungsgemeinschaft. We are grateful to the Verband der Chemischen Industrie for granting a Kekule-scholarship.

REFERENCES

1 Kulicke, W.-M. and Kniewske, R. *Makromol. Chem.* 1981, **182,** 2277
2 Bouldin, M., Kulicke, W.-M. and Kehler, H. *Coll. Polym. Sci.* 1988, **266,** 793
3 Kulicke, W.-M. *Polym. Prepr.* 1989, **30/2,** 379
4 Oertel, R. and Kulicke, W.-M. *Rheol. Acta* 1991, **30,** 140
5 Kulicke, W.-M., Griebel, T. and Bouldin, M. *Polymer News* 1991, **16,** 39
6 Griebel, T., Kulicke, W.-M. and Kniewske, R. *J. Getreide, Mehl Brot* 1992, **5,** 154
7 Kniewske, R. and Kulicke, W.-M. *Makromol. Chem.* 1983, **184,** 2173
8 Kulicke, W.-M. (Ed.), 'Fließverhalten von Stoffen und Stoffgemischen', Hüthig & Wepf, Heidelberg, 1986
9 Flory, P. J. 'Principles of Polymer Chemistry', Cornell, Ithaca, 1953
10 Elias, H.-G. 'Makromoleküle', Hüthig & Wepf, Heidelberg, 1990
11 Lechner, M. D., Gehrke, K. and Nordmeier, E. H. 'Makromolekulare Chemie', Birkhäuser, Basel, 1993
12 Mittelbach, *P. Acta Phys. Austriaca* 1964, **19,** 53
13 Perrin, F. *J. Physique Radium* 1936, **7,** 1
14 Dondos, A. and Papanagopoulos, D. *Polymer* 1995, **36,** 365
15 Dondos, A. and Papanagopoulos D. *Polymer* 1995, **36,** 369.
16 Akcasu, A. Z. *Polymer* 1981, **22,** 1169
17 Akcasu, A. Z., Benmouna, M. and Alkhafaji, S. *Macromolecules* 1981, **14,** 147
18 Burchard, W. *Adv. Polym Sci.* 1983, **48,** 1
19 Buliga, G. S. and Brant, D. A. *Int. J. Biol. Macromol.* 1987, **9,** 71
20 Buliga, G. S. and Brandt, D. A. *Int. J. Biol. Macromol.* 1987, **9,** 77
21 Roessner, D. and Kulicke, W.-M. *J. Chromatogr. A* 1994, **687,** 249
22 Thielking, H., Roessner, D. and Kulicke, W.-M. *Analyt Chem.* 1995, **67,** 3229
23 Thielking, H. and Kulicke, W.-M. *Analyt. Chem.* 1996, **68,** 1169
24 Tsujisaka, Y. and Mitsuhashi, M. in 'Industrial Gums' (Eds R. L. Whistler and J. N. B. Miller, Academic Press, London, 1993, pp. 447–460
25 Giddings, J. C., Lin G. C. and Myers M. N. *J. Liq. Chromatogr.* 1978, **1,** 1–20
26 Brimhall, S. L., Myers, M. N., Caldwell, K. D. and Giddings, J. C. *J. Polym. Sci., Polym. Lett. Edn* 1984, **22,** 339
27 Benincasa, M. A. and Giddings, J. C. *Analyt. Chem.* 1992, **64,** 790
28 Kratochvil, P. 'Classical Light Scattering from Polymer Solutions', Elsevier, Amsterdam, 1987
29 Reed, W. F. *Macromol. Chem. Phys.* 1995, **196,** 1539
30 Nordmeier, E. *J. Phys. Chem.* 1993, **97,** 5770
31 Douglas, J. F. and Freed, K. F. *Macromolecules* 1994, **27,** 6088
32 McCrackin, F. L., Guttman, C. M. and Akcasu, A. Z. *Macromolecules* 1984, **17,** 604
33 Wyatt, P. J. *Anal. Chim. Acta* 1993, **272,** 1
34 Kato, T., Katsuki, T. and Takahashi, A. *Macromolecules* 1984, **17,** 1726
35 Pavlov, G. M., Korneeva, E. V. and Yevlampieva, N. P. *Int. J. Biol. Macromol.* 1994, **16,** 318
36 Peterlin, A. *Makromol. Chem.* 1953, **9,** 244
37 Guttman, C. M., McCrackin, F. L. and Han, C. C. *Macromolecules* 1982, **15,** 1205
38 Schmidt, M. and Burchard, W. *Macromolecules* 1981, **14,** 210
39 Einstein, A. *Ann. Phys.* 1906, **19,** 289
40 Einstein, A. *Ann. Phys.* 1911, **34,** 591
41 Wolff, C. *Eur. Polym. J.* 1977, **13,** 739
42 Brostow, W., Drewniak, M. and Medvedev, N. N. *Macromol. Theory Simul.* 1995, **4,** 745
43 Caldwell, K. D., Brimhall, S. L., Gao, Y. and Giddings, J. C. *J. Appl. Polym. Sci.* 1988, **36,** 703